Published in final edited form as:
Cell Death Differ. 2010 October ; 17(10): 1551–1565. doi:10.1038/cdd.2010.32.

Cytoplasmic polyadenylation element binding protein is a conserved target of tumor suppressor *HRPT2/CDC73*

Jian-Hua Zhang[1,*], **Leelamma M. Panicker**[1,*], **Erica M. Seigneur**[1], **Ling Lin**[1,†], **Carrie D. House**[1,§], **Wynne Morgan**[1,‡], **Weiping C. Chen**[2], **Hina Mehta**[1], **Mayce Haj-Ali**[1], **Zhu-Xi Yu**[3], and **William F. Simonds**[1,£]

[1]Metabolic Diseases Branch, Bldg. 10/ Rm 8C-101, National Institute of Diabetes and Digestive and Kidney Diseases, Bethesda, MD 20892

[2]Genomics Core Laboratory, Bldg. 8/ Rm 1A-11, National Institute of Diabetes and Digestive and Kidney Diseases, Bethesda, MD 20892

[3]Genetics & Development Biology Center, Bldg.14E/ Rm 107D, National Heart, Lung, and Blood Institute, National Institutes of Health, Bethesda, MD 20892

Abstract

Parafibromin, a tumor suppressor protein encoded by *HRPT2/CDC73* and implicated in parathyroid cancer and the hyperparathyroidism-jaw tumor familial cancer syndrome, is part of the PAF1 transcriptional regulatory complex. Parafibromin has been implicated in apoptosis and growth arrest, but the mechanism by which its loss of function promotes neoplasia is poorly understood. We report here that a hypomorphic allele of *hyrax (hyx)*, the *Drosophila* homolog of *HRPT2/CDC73*, rescues the loss-of-ventral-eye phenotype of *lobe (Akt1s1)*. Such rescue is consistent with previous reports that hyx/ parafibromin is required for the nuclear transduction of Wingless/Wnt signals and that Wingless signaling antagonizes *lobe* function. A screen employing double *hyx/lobe* heterozygotes identified an additional interaction with *orb* and *orb2*, homologs of mammalian cytoplasmic polyadenylation element binding protein (CPEB), a translational regulatory protein. *Hyx* and *orb2* heterozygotes lived longer and were more resistant to starvation than controls. In mammalian cells knockdown of parafibromin expression reduced levels of *CPEB1*. Chromatin immunoprecipitation demonstrated occupancy of *CPEB1* by endogenous parafibromin. Bioinformatic analysis revealed a significant overlap between human transcripts potentially regulated by parafibromin and CPEB. These results show that parafibromin may exert both transcriptional and, through CPEB, translational control over a subset of target genes and that loss of parafibromin (and CPEB) function may promote tumorigenesis in part by conferring resistance to nutritional stress.

Keywords

Akt1S1; Longevity; Paf1 complex; Parafibromin; PRAS40

£Corresponding author: William F. Simonds: wfs@helix.nih.gov, Tel: 301-496-9299, Fax: 301-402-0374.
†Present address: Division of Oncology/Hematology, Department of Medicine, Lombardi Cancer Center, Georgetown University School of Medicine, Preclinical Science Building, LF-09, 3900 Reservoir RD NW, Washington, DC 20057; Tel: 202-687-0365
§Present address: Department of Pharmacology and Physiology, George Washington University, Ross Hall Suite 603, 2300 Eye Street NW, Washington, D.C. 20037; Tel: (202) 994-2924
‡Present address: University of Massachusetts Medical School, 55 Lake Ave, Worcester, MA 01605; Wynne.Morgan@umassmed.edu
*These authors contributed equally to this work.

Conflict of Interest

None of the authors has a conflict of interest that could be perceived as prejudicing the impartiality of the research reported herein.

Introduction

Mutation of the tumor suppressor gene *HRPT2/CDC73* in the germline confers susceptibility to the hyperparathyroidism-jaw tumor syndrome (HPT-JT), an autosomal dominant familial cancer syndrome with a high incidence of parathyroid malignancy (1–6). Carpten *et al* identified *HRPT2* by positional candidate cloning (7). Somatic and/or germline inactivating *HRPT2/CDC73* mutations have also been strongly implicated in sporadic parathyroid cancer (8, 9). *HRPT2/CDC73* encodes parafibromin, a 531-amino acid putative tumor suppressor protein with sequence homology to Cdc73p, a yeast protein component of the RNA polymerase II-associated Paf1 complex. Recent evidence suggests that in humans parafibromin also interacts with RNA polymerase II as part of a PAF1 complex (10–12). The components of the PAF1 complex are highly conserved in *Drosophila* as well, including *hyrax* (*hyx*) a homolog of *HRPT2* and *CDC73* (13).

Despite its identification as a component of the PAF1 complex, the key molecular mechanisms by which loss of parafibromin function promotes tumorigenesis remain unclear. Endogenous parafibromin promotes apoptosis (14), and transfected parafibromin inhibits cellular proliferation (15, 16) and induces cell cycle arrest in the G1 phase (16). While these cell biological properties of parafibromin are consistent with its proposed function as a tumor suppressor, few relevant parafibromin target genes or pathways have been identified so far (17, 18). The observation, first made in *Drosophila*, that hyx/parafibromin binds directly to armadillo/β-catenin and facilitates Wingless (Wg)/Wnt signaling (13) has so far not given insight into the critical pathway(s) in which loss of parafibromin function leads to tumor development.

In this study we employ *Drosophila* as a model system to identify a genetic interaction between *hyx* and *orb*, a homolog of mammalian cytoplasmic polyadenylation element binding protein (CPEB). Flies heterozygous for *hyx* or *orb* showed enhanced longevity and marked starvation resistance. In cultured human cells RNA interference with parafibromin expression reduced the expression of *CPEB1* transcript. Chromatin immunoprecipitation (ChIP) experiments demonstrated a direct association of endogenous parafibromin and other PAF1 complex components with *CPEB1*. Thus parafibromin may exert not only transcriptional but, through a conserved interaction with CPEB, translational control over a significant subset of its target genes.

Results

The *hyrax/HRPT2* gene is essential in *Drosophila* development

The significance of the *hyx* gene in *Drosophila* development was assessed using the hypomorphic mutant hyx^{EY6898}. Survey of approximately 300 embryos revealed that $hyx^{EY6898/EY6898}$ embryos had a developmental delay and a reduced hatching rate (22% of w^{1118} control embryos). Heterozygous mutant flies developed normally without obvious morphological defects but homozygotes died at early instars. Staged examination of larval development revealed that $hyx^{EY6898/EY6898}$ larvae developed more slowly than both heterozygotes and w^{1118} control larvae. At about 48 hr after hatching, the $hyx^{EY6898/EY6898}$ larvae were 1/3 the size of the $dhyx^{EY6898/+}$ and w^{1118} controls (Fig. 1, A–C). All of the $hyx^{EY6898/EY6898}$ larvae died at or before second instar. Sectioning of the 48 hr old larvae suggested that the $hyx^{EY6898/EY6898}$ larvae developed disproportionately (Fig. 1D).

In order to verify whether the hypomorphic *hyx* allele was the sole cause of the observed phenotype, we first examined the *hyx* gene transcript levels by quantitative RT-PCR. Compared to comparably developed $hyx^{+/+}$ control flies, the *hyx* mRNA was approximately 55% lower in $hyx^{EY6898/EY6898}$ larvae (Fig. 1E) and 26% lower in $hyx^{EY6898/+}$ adult flies

(Fig. 1F). Precise excision of the P element in $hyx^{EY6898/+}$ flies by remobilization using a jumper line brought the *hyx* gene expression to the level of wild type and rescued the homozygous lethality (not shown). Furthermore the $hyx^{EY6898/EY6898}$ lethal phenotype was partially rescued by overexpression of the *hyx* gene in the $hyx^{EY6898/EY6898}$ background through genotype synthesis (19) and the UAS/GAL4 binary expression system (Fig. 1G, H.). In the presence of the 5C-actin promoter controlled GAL4 expression (*act-GAL4*), approximately 15% of the *act-GAL4*/+;$hyx^{EY6898/EY6898}$ flies developed into adults while no $hyx^{EY6898/EY6898}$ did (Fig. 1G, H).

Other mutant *hyx* alleles were tested and the penetrance of the lethality phenotype correlated inversely with the level of *hyx* gene expression. The $hyx^{dEY2/+}$ fly was created by imprecise excision of the P-element from $hyx^{EY6898/+}$. Quantitative RT-PCR analysis revealed that there was about a 40% reduction in *hyx* mRNA in $hyx^{dEY2/dEY2}$ larvae versus w^{1118} controls, while three homozygous *hyx* deficiency mutants (hyx^{ED5301}, hyx^{ED5331}, hyx^{ED5343}) had undetectable *hyx* mRNA (data not shown). Although heterozygotes of all four mutants developed normally, homozygotes of the three *hyx* deficiency mutants died at a late embryo stage before hatching, much earlier than $hyx^{EY6898/EY6898}$ flies, while the homozygotes of the imprecise excision mutant ($hyx^{dEY2/dEY2}$) died in late third instar, later than the $hyx^{EY6898/EY6898}$ flies. Like hyx^{EY6898} homozygotes, $hyx^{dEY2/dEY2}$ adult flies were never found in the F1 generation of $hyx^{dEY2/+}$ matings (Fig. 1H). These results confirmed the critical role of the *hyx/HRPT2* gene in fly development and the GAL4-mediated partial rescue of the early larval lethality of $hyx^{EY6898/EY6898}$ previously described (13).

Phenotype screening identifies *orb/orb2* as *hyx/HRPT2* interacting genes

Screening for *hyx* suppressors or enhancers was performed by crossing $hyx^{EY6898/+}$ mutants with approximately 400 selected mutant fly stocks. The fly stocks chosen for screening contained mutant alleles of fly genes homologous to human genes implicated in oncogenic, tumor suppressor or stress resistance pathways. New phenotypes distinctive from either parent were identified. It was found that doubly heterozygous mutants of *hyx* and *lobe (L)* (the homolog of mammalian Akt1 substrate1 [AKT1S1] also called the proline-rich Akt substrate of 40 kDa [PRAS40]), (L^{si}/+;hyx^{EY6898}/+), had normal eyes like $hyx^{+/+}$ and $hyx^{EY6898/+}$ flies (Fig. 2F, cf. 2A,B), even though heterozygous $L^{si/+}$ flies had a loss-of-ventral-eye phenotype (Fig. 2C) (20). Thus *hyx/HRPT2* could suppress or rescue the L^{si} phenotype. Rescue of the half eye phenotype was confirmed by crossing hyx^{EY6898}/+ flies with other mutant alleles of *L*. The half eye *L* mutant phenotype was rescued in all of the *L* and *hyx* double heterozygous flies generated (L^{1}/+;hyx^{EY6898}/+, L^{2}/+;hyx^{EY6898}/+, L^{4}/+;hyx^{EY6898}/+, L^{5}/+;hyx^{EY6898}/+, L^{r}/+;hyx^{EY6898}/+) (not shown).

The basis of the genetic interaction observed between *hyx/HRPT2* and *lobe* is unknown. Since L^{si} is a likely dominant negative mutation with high penetrance (21) and $hyx^{EY6898/+}$ heterozygotes had no obvious morphological phenotype, we hypothesized that the combination of the $L^{si/+}$ and $hyx^{EY6898/+}$ mutations might sensitize the genetic background to allow rapid identification of genes that interact with *L* or *hyx/HRPT2* or both. To explore this possibility we employed a doubly heterozygous mutant fly line (L^{si}/*cyo;* hyx^{EY6898}/*Tm3*) generated by genotype synthesis (19). We first tested the hypothesis by crossing the *lobe/hyx* double heterozygotes with strains carrying mutations of PAF1 complex component genes besides *hyx*, expected to interfere with the rescue of *L* by *hyx*.

To this end the doubly heterozygous mutant fly (L^{si}/+; hyx^{EY6898}/+) was crossed with fly strains harboring mutations in PAF1 complex component homologs, including *atms/paf1*(CG2503), *atu/leo1*(CG1433) and *dctr9* (CG9899) genes (Table I, crosses 11–14). The triply heterozygous flies L^{si}/+;hyx^{EY6898}/atu^{s1938}/+ and L^{si}/+;hyx^{EY6898}/$dctr9^{NP5197}$/+ had a high percentage of flies with a distinctive, novel eye phenotype ranging from notched

ventral eye field with small overgrowths to a half eye with large dysplastic overgrowths present in the missing ventral eye region (NOG phenotype) (Table I, crosses 11,14). In contrast, doubly heterozygous offspring from the same crosses with genotypes $L^{si}/+;atu^{10217}/+$ *and* $L^{si}/dctr9^{NP5197}$ had normal eyes (Table I, crosses 11,14). Two mutant alleles of the *Paf1* homolog *atms* were employed, $atms^{NP5451}$ and $atms^{rk509}$. Both the $L^{si}/+;hyx^{EY6898}/atms^{NP5451}$ and the $L^{si}/+;hyx^{EY6898}/atms^{rk509}$ triply heterozygous offspring expressed the NOG phenotype but the latter had a higher penetrance (Table I, crosses 12,13). However some ~20% of the $L^{324}/+;atms^{rk509}/+$ double heterozygotes also had NOG eyes, indicating there might be a *hyx*-independent interaction between *atms/Paf1* and L^{si} genes (Table I, cross 13). Similarly, genetic interaction evidenced by the NOG phenotype was also observed between $L^{si}/+;hyx^{EY6898}/+$ and the *Armadillo(Arm)/β-catenin* genes (Table I, cross 20) (13).

Using the same strategy we crossed the doubly heterozygous ($L^{si}/+;\ hyx^{EY6898}/+$) flies with other individual heterozygous flies from the collection of stock mutants strains to screen for new genetically interacting genes. The genetically interacting genes were defined as those that produced novel eye phenotypes in one of three possible triple heterozygous genotypes: $+/+;\ L^{si}/X;\ hyx^{EY6898}/+$ or $+/+;\ L^{si}/+;\ hyx^{EY6898}/X$ or $X/+;\ L^{si}/+;\ hyx^{EY6898}/+$, where *X* was the tested gene mutant. Approximately 5% of the ~400 screened gene mutant strains produced abnormal eye phenotypes (see below, and manuscript in preparation).

Crosses of $L^{si}/+;\ hyx^{EY6898}/+$ double heterozygotes with flies harboring a mutant allele of the cytoplasmic polyadenylation element binding protein (*CPEB*) homolog *orb2*, $orb2^{BG02373}$, produced offspring with a high frequency of the NOG phenotype (Fig. 2H, I, K). CPEB is an RNA-binding zinc-finger protein that controls the cytoplasmic polyadenylation of certain mRNAs and can repress or mask the their translation (22). Approximately 25% of the triple heterozygotes ($L^{si}/+;hyx^{EY6898}/orb2^{BG02373}$) flies had NOG eye phenotypes including half eye with large overgrowths in the missing ventral eye region (Fig. 2H, I, K; Table I, cross 4). Although the dysplastic tissue frequently had a recognizable eye-like arrangement, the ommatidia and sensory bristles were deformed and in disarray (Fig. 2K, cf. 2J). Testing of two other *orb2* mutant alleles gave similar results (Table I, crosses 5, 6). Although crossing the $L^{si}/+;\ hyx^{EY6898}/+$ double heterozygotes with the *orb* gene mutants did produce a similar NOG phenotype, the penetrance was lower than that seen in the *orb2* crosses (Table I, crosses 7–10). In contrast ~95% of the doubly heterozygous mutant flies ($L^{si}/+;orb2^{BG02373/+}$, $L^{si}/+;orb^{dec}$, $L^{si}/+;hyx^{EY6898/+}$, $hyx^{EY6898}/orb2^{BG02373/+}$ and hyx^{EY6898}/orb^{dec}) had normal eyes (Fig. 2E, F; Table I, crosses 4–7). These interactions were further confirmed by similar interactions of $L^{si}/+;hyx^{EY6898/+}$ with the deficiency mutants of both *orb2* and *orb* (Table I, crosses 5,6,9,10). Because all other possible doubly heterozygous mutants from the same matings produced flies with normal eyes (Table I, crosses 5,6,9,10), the observed NOG eye phenotype must be from the specific combination of *hyx* and *orb* loss of function. As noted above, the triply heterozygous $L^{si}/+;hyx^{EY6898}/orb2$ mutant flies produced significantly larger overgrowths and exhibited higher penetrance of the NOG phenotype than the $L^{si}/+;hyx^{EY6898}/orb$ flies, suggesting a stronger interaction of *hyx* with the *orb2* alleles.

Because the doubly heterozygous mutant flies ($L^{si}/+;hyx^{EY6898}/+$) only genetically interacted with ~5% of our collection of mutant fly stocks, it is reasonable to believe that the genetic interactions with *orb* and *orb2* are specific. To further assess the selectivity of the interactions, we also tested to see if the $L^{si}/+;hyx^{EY6898}/+$ double heterozygotes interacted with the *foxo* and *4EBP* genes (Table I, crosses 21–30). Like *L/akt1s1*, Foxo is a downstream target of the *akt* gene. The protein 4EBP competes with eIF-4G for binding to eIF-4E to regulate translational initiation (23), a process that CPEB can also regulate through interaction with the eIF-4E-binding protein Maskin (24). The $L^{si}/+;hyx^{EY6898}/+$

flies were crossed with six mutants of *foxo* and four mutants of *thor* (*4EBP* homolog). No genetic interactions were observed among the resulting triply heterozygous flies (Table I, crosses 21–30).

The eye phenotype in $L^{si}/+;hyx^{EY6898}/orb2^{BG02373}$ triple heterozygotes is associated with an abnormal pattern of apoptosis and increased ectopic cell proliferation in larval eye discs

The NOG phenotype observed in the $L^{si}/+;hyx^{EY6898/+}/orb2^{BG02373/+}$ triple heterozygotes could result from either impaired apoptosis and/or excessive proliferation during eye development. The imaginal discs of third instar larvae of wild-type and $L^{si}/+;hyx^{EY6898/+}/orb2^{BG02373/+}$ triple heterozygote flies were therefore examined using the TUNEL assay to identify the nuclei of cells undergoing apoptosis, and compared to discs of $L^{si}/+$ larvae, since loss of *L* has been shown to induce apoptosis at this stage (20), as well as to discs from larvae from the three double heterozygote combinations and the other single heterozygotes (Fig. 3A–C). In the developing imaginal disc, the morphogenetic furrow (MF) moves across the eye field in the posterior to anterior direction, inducing differentiation in the cells directly posterior to it (25). The majority of TUNEL-positive apoptotic cell nuclei in the eye imaginal discs of wild-type, $hyx^{EY6898/+}$, $orb2^{BG02373/+}$, and double heterozygote $hyx^{EY6898/+};orb2^{BG02373/+}$ eye discs are located posterior to the MF and uniformly distributed whereas the majority of apoptotic nuclei in the $L^{si}/+$ single heterozygotes and $L^{si}/+$; $hyx^{EY6898/+}/orb2^{BG02373/+}$ triple heterozygotes are found anterior to the MF and grouped in large clusters (Fig. 3A, B). The majority of apoptotic nuclei in the $L^{si}/+$; $hyx^{EY6898/+}$ double heterozygotes are also localized anterior to the MF, but are dispersed rather than grouped. There was no significant difference with respect to the MF in the location of apoptotic nuclei in $L^{si}/+$; $orb2^{BG02373/+}$ double heterozygotes (Fig. 3A, B). The total number of TUNEL-positive apoptotic nuclei per entire eye imaginal disc of $L^{si}/+$ heterozygote larvae was significantly greater than either w^{1118} control, triple, double, or other single heterozygote larvae (Fig. 3C). Cell proliferation in the larval eye discs was assayed by the incorporation of the synthetic nucleoside 5-ethynyl-2´-deoxyuridine (EdU) into newly synthesized DNA. In wild-type larvae, EdU incorporation was evenly distributed anterior to the MF, where cells are cycling asynchronously, and was slightly more intense just posterior to the MF, where cells are undergoing synchronous S phase (Fig. 3D). In the $L^{si}/+$; $hyx^{EY6898}/orb2^{BG02373}$ triple heterozygotes, staining for EdU incorporation frequently revealed bright clusters of proliferating cells anterior to the MF suggesting an increase in ectopic cellular proliferation. Thus the developing eye discs of $L^{si}/+$; $hyx^{EY6898}/orb2^{BG02373}$ triple heterozygotes with a propensity to later develop the NOG phenotype were characterized by both an abnormal pattern of apoptosis and an increased incidence of ectopic cellular proliferation.

The *hyx/HRPT2* and *orb2* genes regulate fly lifespan and starvation resistance

HRPT2/CDC73 is a putative tumor suppressor gene (7). Well characterized tumor suppressor genes like *P53* and *Rb* have been implicated in the processes of cellular senescence, longevity and stress resistance (26). In addition CPEB has been shown to regulate cellular senescence in mouse embryonic fibroblasts (22). We therefore tested if *hyx/HRPT2* and/or *orb2* might control longevity and stress resistance in the present fly model. Flies heterozygous for *hyx/HRPT2* or *orb2* had significantly enhanced longevity compared to w^{1118} control flies (Fig. 4A, B). Since longer lifespan is often associated with enhanced stress resistance in fly, we tested if oxidative stress resistance was a factor causing longer lifespan in both *hyx/HRPT2* and *orb2* heterozygous mutants. However no significant differences in resistance to paraquat (an *in vivo* free radical generator) treatment were observed, suggesting that oxidative stress is not the cause of the extended lifespan (Fig. 4C).

Resistance to starvation however was found to be significantly higher in both *hyx/HRPT2* (*hyx*^{EY6898}/+) and *orb2* (*orb2*^{BG2373}/+) heterozygous flies compared to controls (Fig. 4D–E). To prove that the *hyx/HRPT2* mutation was the cause of the extended lifespan phenotype, we tested for rescue of the phenotype upon overexpression of the *hyx/HRPT2* gene on the *hyx*^{EY6898} allele in *act-GAL4*/+;*hyx*$^{EY6898/+}$ flies. As shown in Fig. 4F, overexpression of *hyx/HRPT2* gene restored starvation sensitivity to near control levels, whereas flies with 5C-actin promoter-driven GAL4 expression only (but lacking the GAL4-sensitive *hyx*^{EY6898} allele) had slightly enhanced starvation resistance (Fig. 4G). Note that the incomplete rescue of the lethality phenotype by actin GAL4-driven *hyx/HRPT2* expression documented in Fig. 1H was against a *hyx*$^{EY6898/\,EY6898}$ background whereas the full rescue of the starvation resistance phenotype by actin GAL4-driven *hyx/HRPT2* overexpression in Fig. 4F was in the context of *hyx*$^{EY6898/+}$ flies. Furthermore, flies doubly heterozygous for *hyx/HRPT2* and *orb2* (*hyx*$^{EY6898/+}$/ orb2$^{BG2373/+}$) showed starvation resistance similar to the *hyx*$^{EY6898/+}$ flies (Fig. 4H, cf. 4D). Doubly heterozygous *hyx*$^{EY6898/+}$/ orb2$^{BG2373/+}$ flies with 5C-actin promoter-driven GAL4 overexpression of *hyx/HRPT2* from the *hyx*^{EY6898} allele exhibited starvation resistance comparable to control flies (Fig. 4I, cf. 4H), suggesting that *hyx/HRPT2* gene overexpression could also blunt the effects of *orb2*.

Hyrax/HRPT2 functions upstream of *orb2*

The genetic interaction between *hyx/HRPT2* and *orb2* observed in the eye phenotypes of the *L* triple heterozygotes, as well as the lack of synergy in the lifespan and starvation resistance experiments, suggest that *hyx/HRPT2* and *orb2* function in the same pathway, but provide no insight into the relative position of the two genes. To understand their functional relationship better, quantitative RT-PCR was used to measure transcript levels of the genes in fly strains carrying mutant alleles for *hyx/HRPT2* or *orb2*. Levels of *orb2* transcript were reduced by some 80% in larvae of *hyx*^{EY6898} homozygotes and by 25% in adult *hyx*^{EY6898} heterozygotes compared to control (Fig. 1I, J). In contrast, adult flies homozygous for *orb2*^{BG02373} had normal levels of *hyx/HRPT2* transcript (Fig. 1M) even though *orb2* message levels were successively reduced in heterozygous and homozygous *orb2*^{BG02373} flies (Fig. 1K, L). Taken together these results indicate *hyx/HRPT2* functions upstream of *orb2* acting at least in part at the transcriptional level.

Parafibromin regulates the transcription of CPEB isoforms in mammalian cells

Hyx and parafibromin represent a family of gene products widely conserved among eukaryotes as components of Paf1/PAF1 complexes. We therefore examined mammalian cells for evidence of a conserved pathway connecting *HRPT2/CDC73* and *CPEB* comparable to that between *hyx/HRPT2* and *orb2*. To study this we employed RNA interference to impair the expression of parafibromin and Paf1 (14, 17). Transfection of HEK-293FT cells with small interfering duplex RNAs (siRNA) targeting two different sequences of the *HRPT2/CDC73* or *Paf1* transcripts inhibited the expression of their target genes compared to scrambled siRNA (Ctrl) or siRNA targeting the unrelated gene Gβ5, as evidenced by quantitative immunoblotting (Fig. 5A,B). Knockdown of parafibromin expression also impaired the expression of Paf1 in these cells (Fig. 5B). RNA interference employing *HRPT2*- and *Paf1*-targeted siRNAs was therefore used to study the effect of parafibromin and Paf1 knockdown on mammalian *CPEB* expression.

There are four CPEB isoforms in mammals, CPEB1-4. RNA interference targeting the *HRPT2/CDC73* transcript knocked down *HRPT2/CDC73* transcript levels, as expected (Fig. 5C), and significantly diminished the expression of *CPEB1* and *CPEB3* but had little effect on *CPEB2* and *CPEB4* (Fig. 5D). If the effects of *HRPT2*/parafibromin knockdown on CPEB involved the former's role as a component of the PAF1 complex, then knocking down Paf1 might also affect *CPEB* gene expression. Reduction of Paf1 gene expression by RNA

interference significantly reduced *CPEB1* and *CPEB4* expression but had no effect on *CPEB2* or *CPEB3* (Fig. 5E). To check if the effects of parafibromin and Paf1 knockdown on *CPEB* expression were redundant or additive, we treated cells with both parafibromin and Paf1 siRNAs and measured the resulting transcript levels of the *CPEB* isoforms (Fig. 5F). Combined interference with both parafibromin and Paf1 expression enhanced the knockdown of *CPEB1* and *CPEB2* expression but had little additional effect on *CPEB3* or *CPEB4* (Fig. 5F). The additivity of effect on *CPEB1* and *CPEB2* transcript levels could argue against the involvement of the PAF1 complex or, since treatment with parafibromin and Paf1 siRNAs only partially knocked down expression of their cognate proteins (see. Fig. 5A, B), may alternatively reflect a synergistic reduction of PAF1 complex expression and function when both parafibromin and Paf1 siRNAs were employed. Taken together, these results suggested that while parafibromin and Paf1 co-regulate *CPEB1* gene expression through a mechanism that may involve the PAF1 complex, regulation of CPEB3 and CPEB4 gene expression might be through alternative pathways.

Quantitative immunoblots of parafibromin and CPEB1 were performed after RNA interference with parafibromin expression using siRNAs targeting three different regions of the *HRPT2/CDC73* transcript (Fig. 5G, H). All three *HRPT2/CDC73*-directed siRNAs reduced parafibromin expression and also knocked down CPEB1 protein levels, with the most effective reagent being the sipfb-1 siRNA (Fig. 5G, H). To test the specificity of the RNA interference, silent base changes designed to impair interaction with sipfb-1 siRNA were introduced into a cDNA encoding an AU5-epitope-tagged human parafibromin and a rescue experiment performed (Fig. 5I). Whereas *CPEB1* expression was knocked down by sipfb-1 siRNA treatment it was rescued by transfection of siRNA-resistant AU5-parafibromin, but not wild-type AU5-parafibromin (Fig. 5I). Rescue of *CPEB1* expression was seen with two other siRNA-resistant AU5-parafibromin mutants with different silent base changes (not shown). The sipfb-1 siRNA treatment was effective at impairing the expression of both endogenous parafibromin and transfected wild-type AU5-parafibromin (with slightly slower mobility on SDS-PAGE due to the epitope tag), but consistently enhanced expression of the siRNA-resistant AU5-parafibromin (Fig. 5I, parafibromin immunoblot panel, cf. lanes 5,6 vs. lanes 1,2 and 3,4). We speculate that this paradoxical effect may be due to increased stability of the AU5-parafibromin protein encoded by the siRNA-resistant cDNA when it is able to complex with other PAF1 complex components, an ability that is enhanced when competing endogenous parafibromin is knocked down.

Parafibromin and other PAF1 complex components bind to the CPEB1 gene

Knockdown of parafibromin reduced *CPEB1* mRNA and protein levels. ChIP was used to determine if this effect was consistent with regulation at the transcriptional level. Six pairs of primers were used to interrogate anti-parafibromin immunoprecipitates in the ChIP assay by quantitative PCR, three sets targeting regions upstream of the *CPEB1* transcriptional start site (U1, U2, and U3), two sets targeting internal gene coding sequences (S and M), and one set directed at a region 1100 bp downstream of the *CPEB1* gene (D1) (Fig. 6A). As shown in Fig. 6B, primer pairs U2, S and M produced significantly higher signals from the anti-parafibromin immunoprecipitates than from those using control IgG. ChIP assays employing antibodies to other components of the PAF1 complex, Paf1 and Leo1, also gave strong specific signals with the U2, S and M primer pairs targeting *CPEB1* (Fig. 6C–D). The specific ChIP signal was much stronger in the U2, U1, and D1 regions of *CPEB1* than in the U3 region (Fig. 6E). Taken together, these data suggest that the PAF1 complex might be involved in both *CPEB1* transcript initiation and elongation, consistent with PAF1 function at other gene loci (10–12, 27) and the observation above that Paf1 knockdown reduced *CPEB1* transcript levels (Fig. 5E).

In contrast, none of the parafibromin, Paf1 and Leo1 specific antibodies yielded specific signal when interrogated with primers to the *CPEB3* gene (Fig. 6F). These results suggest that parafibromin and the PAF1 complex play a direct regulatory role in the transcription of *CPEB1* but not *CPEB3*, consistent with the failure of siRNA-mediated knockdown of Paf1 to affect *CPEB3* transcript levels shown above (Fig. 5E).

Bioinformatic analysis of potential CPEB1 and *hyx/HRPT2* target genes

The regulation of *CPEB1* gene transcription by *HRPT2/CDC73* implies that parafibromin, apart from its transcriptional regulatory role as part of the PAF1 complex, might affect the translation of some genes indirectly through its regulation of CPEB1. In order to estimate the set of potential target genes regulated by both *HRPT2/CDC73* and *CPEB1* genes we performed a bioinformatic analysis. Whole genome microarray analysis was used to identify potential *HRPT2/CDC73* target genes. In HEK293 cells there were 2117 genes whose transcription levels were either decreased or increased in response to RNA interference with, or cDNA transfection-mediated enhancement of, the expression of *HRPT2/CDC73* (not shown). Potential *CPEB1* target genes were identified by whole transcriptosome analysis using a computer program to identify transcripts with canonical CPE signals ($U_{4–5}A_{1–2}U$) located at an appropriate distance upstream of the poly(A) signal (AAUAAA) in their 3' untranslated regions. This software analysis identified 3921 gene transcripts, a set that included known CPEB targets such as cyclin B1, c-Myc, and cdk1 (not shown). Comparison of the sets of potential *HRPT2/CDC73* and *CPEB1* target genes revealed 311 common genes, approximately 15% of the *HRPT2/CDC73* targets (Supplemental Table I). To gauge the significance of this overlap, the sets of potential *HRPT2/CDC73* and *CPEB* target genes were compared to a set of >3000 randomly selected genes. The overlap between the random set and the *HRPT2/CDC73* and *CPEB* target sets was 2 and 3% respectively (Fig. 7A). The overlap of potential *HRPT2/CDC73* and *CPEB* target gene sets is therefore highly significant (Fisher's exact test, 2-tailed p value < 0.002, *HRPT2/CPEB* vs. *HRPT2*/Random; < 0.01, *CPEB/HRPT2* vs. *CPEB*/Random).

Discussion

Tumor suppressor genes generally induce programmed death or growth arrest (senescence) in cells malfunctioning because of genotoxic, oxidative, or nutritional stress, thus minimizing the deleterious effects of the cell on its neighbors (28, 29). The putative tumor suppressor gene *HRPT2/CDC73* can induce growth arrest and apoptosis *in vitro* (14, 16) and in the present study we demonstrate an evolutionarily conserved pathway linking *hyx/HRPT2* and *orb2/CPEB* and show that loss of function of either gene enhances starvation resistance and increases lifespan in a fly model.

The control of *orb/CPEB* gene expression by *hyx/HRPT2* expands the potential mechanisms by which the tumor suppressor gene can control the expression of its targets (Fig. 7B). CPEB is a kinase-regulated RNA-binding protein component of the eIF-4E translation initiation complex that can regulate translation by either repressing or facilitating the cytoplasmic polyadenylation of a subset of 5' capped mRNAs (24, 30). CPEB has been previously implicated in the regulation of cell proliferation and senescence (22), effects that may involve the translational regulation of tumor suppressor *P53* expression (31). The bioinformatic analysis presented here suggests that the potential targets of the *HRPT2/CDC73* include a subset of genes subject to both transcriptional and, through CPEB, translational control (Type III targets in Fig. 7B). Although the dual regulation of these putative target genes awaits experimental validation, it is tempting to think that *HRPT2/CDC73* may exercise its tumor suppressor functions by utilizing a repertoire of distinct but reinforcing control mechanisms. The *MYC* protooncogene, for example, is repressed by parafibromin at both the transcriptional level and by a mechanism involving destabilization

at the protein level (17). The potential for a third mechanism of control must now be considered since *MYC* is a target of CPEB (22) and was indeed identified as a potential target of both *HRPT2/CDC73* and *CPEB* in the present bioinformatic analysis (Supplemental Table I).

Although the linkage between hyx/parafibromin and orb/CPEB demonstrated here is at the transcriptional level other mechanisms must be considered. In budding yeast the Paf1 complex including the parafibromin homolog Cdc73p can directly interact with the 3'-mRNA processing cleavage and polyadenylation factor Cft1 (32). In cultured human cells, multiple subunits of the cleavage and polyadenylation specificity factor (CPSF) as well as the cleavage stimulation factor were recently identified by mass spectroscopy in anti-parafibromin immunoprecipitates (18). Since these immunoprecipitates also contained symplekin (18), a putative scaffolding protein that binds both CPEB and CPSF and is required for CPEB-mediated polyadenylation (33), it is possible that a physical regulatory complex containing parafibromin and CPEB may also exist.

The rescue phenotype of the *lobe/hyx* double heterozygote we report may provide fresh insight into the earlier observation that hyx/parafibromin binds directly to armadillo/β-catenin and facilitates Wg/Wnt signaling (13). Previous studies of the developing *Drosophila* eye showed that *lobe* was required for early cell survival, and that loss of *lobe* function was associated with the induction of cell death and upregulation of Wg signalling (20) and indeed our studies confirm a marked increase in the number of apoptotic nuclei in the eye imaginal discs of L^{si}/+ heterozygote larvae (Fig. 3A, C). Singh *et al* furthermore found that blockade of Wg signaling could rescue the *lobe* loss-of-function phenotype (20). In this light it is tempting to speculate that the rescue of *lobe* loss-of-function in *lobe/hyx* double heterozygotes may reflect the requirement of hyx/parafibromin for nuclear transduction of the Wg/Wnt signal (13).

Two lines of evidence presented here suggest that the tumor suppressor function of hyx/parafibromin may result in part from an involvement in nutritional sensing pathways. First, as discussed above, it was found that *hyx/HRPT2* heterozygosity could rescue the loss of function phenotype of *lobe*, the fly homolog of PRAS40. PRAS40 is a raptor-interacting protein and target of the mTOR kinase that can inhibit cell growth under conditions of nutritional stress (see (34) for recent review). Secondly we observed that heterozygous *hyx/HRPT2* loss of function enhanced fly longevity and imparted resistance to starvation. *Orb2/CPEB* heterozygosity had a similar effect on longevity and nutritional stress resistance. At the cellular level it is clear that heightened resistance to nutritional stress resulting from *hyx/HRPT2* or *orb/CPEB* loss of function would enhance tumorigenesis by promoting the survival of rapidly dividing and hypermetabolic tumor cells as levels of available nutrients decline. Future work will help resolve the critical interactions linking parafibromin to nutrient sensing machinery and other pathways involved in tumorigenesis.

Materials and methods

Fly stocks

The enhancer trapped fly lines from the Japanese NP Consortium Gal4 Enhancer Trap Insertion Database (GETDB) were obtained from Drosophila Genetic Resource Center (DGRC), Kyoto Institute of Technology, Kyoto, Japan. The fly line bearing the hypomorphic allele, hyx^{EY6898}, which contains a P-element (P[EPgy2]) insertion located 36 bp upstream of the *hyx* translational start site in the 5' untranslated transcript region was originally obtained from the Gene Disruption Project (GDP), Baylor College of Medicine, Texas, but is now available from the Bloomington Drosophila Stock Center at Indiana University (Stock No. 16768). The $hyx^{dEY2/+}$ fly was created via imprecise excision of

P[EPgy2] by crossing *hyx*^{EY6898} with the transposase expressing fly line, *Pi(Δ2–3)k* To create the doubly heterozygous mutant fly line (*L*^{si}*/cyo; hyx*^{EY6898}*/Tm3*), standard genotype synthesis methodology employing both the second and third chromosome balancers (*Cyo/Sco* and *Tm6/Tm3*) was used (19). All the other fly lines used were obtained from the Bloomington Drosophila Stock Center at Indiana University.

Morphogenesis, histology and scanning electron microscopy

Fly morphogenesis during development was characterized using stereomicroscopy. Wild type flies and those with different genetic mutations were synchronized developmentally by collecting embryos every hour and examined morphologically at different developmental stages by stereomicroscopy (Zeiss Stemi 2000-C). Detailed structures of fly eyes were further studied using variable pressure vacuum scanning electron microscopy (Hitachi S-3400N VP SEM). Flies were first fixed in 4% paraformaldehyde (Electron Microscopy Sciences) overnight and then maintained in 100% ethanol. Immediately before use, fly heads were removed and examined under appropriate vacuum pressure so that the fly eyes maintained their shapes for 10–15 minutes before deformation. Paraffin-embedded sections of fly larvae were prepared by Histoserv, Inc (Germantown, MD) and examined by standard light microscopy.

Single larva genotyping

In order to create *L*^{si}*/+; hyx*^{EY6898}*/orb2*^{BG02373} triply heterozygous larvae, *L*^{si}*/L*^{si}*; hyx*^{EY6898}*/Tm3* heterozygotes were crossed with *orb2*^{BG02373}*/orb2*^{BG02373} flies. After the mouthpart was removed from each of the resulting third instar larvae, the remainder of the body was put individually into a single well of a 96 well plate containing 50 μl of DirectPCR lysis reagent (Viagen, Cat# 102-T) and incubated at 85 °C for 45 min. PCR reactions were performed using 2 μl of the supernatant and the Brilliant® II SYBR® Green QPCR Master Mix kit (Agilent Technologies) in a 20 μl of total reaction volume. The PCR cycling conditions used were: 95 °C 10’, followed by 40 cycles of 95 °C X 30’’, 55 °C X 1 min, and 72 °C X 1 min. The primer pairs used to detect the wild-type *hyx* gene were: 5’-GAGAAGCGATGCACTCTCTATG-3’and 5’-GCTACGCACTTTGTAATCCGCGAAAG-3’; and for the mutant *hyx* gene were: 5’-CAATCATATCGCTGTCTCACTCA-3’ and 5’-GCTACGCACTTTGTAATCCGCGAAAG-3’.

Larval eye disc apoptosis and cell proliferation analysis

The ApopTag Red *In Situ* Apoptosis Detection Kit (Millipore) was used for TUNEL analysis. Eye discs from third instar larvae were dissected in PBS and fixed in 4% paraformaldehyde for 20 min at RT, washed 3 x in PBTween (5 min ea), post-fixed in pre-cooled 2:1 EtOH:PBS for 5 min at −20° C, and washed 2 X in PBTween (5 min ea). Eye discs were then incubated in 10mM sodium citrate (pH 6.0) for 30 min at 70° C, and rinsed in pure dH_2O for 10 min at RT. Tissue was then incubated in working strength TdT Enzyme (prepared according to manufacturer’s instructions) for 1h at 37° C, incubated in 1X Stop/Wash solution for 10 min at RT, and washed 3 x in PBTween (1 min ea) at RT. Tissue was then incubated in ApopTag anti-digoxigenin with rhodamine for 30 min at RT, protected from the light. Eye discs were then washed 4 x in PBTween (2 min ea) at RT, mounted in Vectashield Mounting Solution with DAPI, and analyzed using fluorescence microscopy. For the detection of cellular proliferation in third instar eye imaginal discs the Click-iT EdU Alexa Fluor 488 Imaging Kit (Invitrogen) was used. Late second instar larvae were collected and fed a 200 μl solution of 20 μM 5-ethynyl-2’-deoxyuridine (EdU) per g of food for 24 hr. Eye discs were then dissected in PBS and fixed in 4% paraformaldehyde for 20min at RT. Eye discs were washed 2 x with PBS, (2 min ea) and incubated in 0.5% Triton X-100 for 30 min at RT. A Click-iT reaction cocktail (containing Alexa 488 azide for the detection of

EdU incorporation) was prepared according to the manufacturer's instructions. Eye discs were incubated in the Click-iT reaction cocktail for 30 min at RT, protected from the light, and then rinsed briefly in Click-iT reaction rinse buffer. Eye discs were then mounted in Vectashield Mounting Solution with DAPI, and analyzed using fluorescence microscopy. Clusters of EdU-positive cells anterior to the morphogenetic furrow were counted in wild-type or triple heterozygote larval eye discs if their brightness exceeded that of the average level in the antennal portion of the imaginal disc, used as an internal reference.

mRNA quantification

Gene expression levels were estimated based on transcript abundance as measured by quantitative RT-PCR and oligo microarray analysis. Quantitative RT-PCR was performed with one step quantitative RT-PCR master mix (Agilent Technologies) using a Stratagene MX 3000P real time PCR machine and analyzed using the accompanying software. For each experiment, β-actin was used for normalization. For every run, standard curves from 4–5 points of 1:4 serial dilutions of both β-actin and the target gene were performed to minimize differences between runs. Each reaction was conducted in triplicate and 3–9 biological samples prepared independently were used in data analysis. The Prism software version 5.0b (GraphPad Software, Inc.) was used for graphing of the analyzed data set. Microarray analysis was performed using the Affymetrix whole genome DNA array. Total RNA was prepared from both treated and control samples using QIAGEN RNeasy kit. RNA probe preparation, hybridization and primary data analysis were performed by the NIH/NIDDK microarray core facility.

Genetic screening for *hyx/HRPT2* gene modifiers

The first phase of genetic screening was conducted using the *hyx/HRPT2* gene P element mutation line EY6898/TM3 and approximately 400 target fly stock lines obtained from either the Bloomington or Japanese GETDB fly stock centers. The target fly lines chosen for screening contained mutant alleles of fly genes homologous to human genes implicated in oncogenic, tumor suppressor or stress resistance pathways. Crosses that produced offspring with altered phenotypes were recorded. The second phase of genetic screening was performed using a triple gene interaction strategy. The doubly heterozygous mutant L^{si}*/cyo;* hyx^{EY6898}*/Tm3* (generated by genotype synthesis as described above) was used to re-screen the 400 target fly lines. Crosses that produced offspring with eye phenotypes different from the parents were recorded. To determine if the novel phenotype resulted from the interaction of the target gene with *lobe* gene or with *hyx/HRPT2* gene, *lobe*/ target gene double heterozygotes and *hyx/HRPT2*/ target gene double heterozygotes were also examined for eye phenotype changes.

Antibodies, mammalian cDNA expression constructs, and cell culture

Antibodies used included goat anti-CPEB (K-16) antibody (sc-48983, Santa Cruz Biotechnology, Santa Cruz, CA), rabbit anti-human parafibromin antibody GRAPE-2 (14), mouse anti-AU5 monoclonal (MMS-135R, Covance Research Products, Denver, PA), mouse anti-β-actin monoclonal (A5316, Sigma, St. Louis, MO), rabbit polyclonal anti-Leo1 (A300-175A, Bethyl Laboratories, Inc., Montgomery, TX) and rabbit polyclonal anti-Paf1 (A300-172A, Bethyl Labs). Secondary antibodies utilized in immunoblots were Cy3-conjugated donkey anti-mouse IgG (715-165-150, Jackson ImmunoResearch Labs, West Grove, PA) and IR secondary antibodies (anti-rabbit IR 800 and anti-mouse Red and Green) from LI-COR Bioscience. RNA interference methodology and the sequences of parafibromin- and Paf1-directed siRNAs were previously described (14, 17). Complementary cDNA for AU5-epitope N-terminally tagged human parafibromin was previously described (15). AU5-tagged human parafibromin cDNA with silent base changes introduced to impair interaction with siRNA construct siPfb-1 was prepared using the

QuickChange II Site-Directed Mutagenesis Kit (Stratagene) and a mutagenic primer pair consisting of the sense primer 5'-CAG ACT GAA CAG ATT AGG agc cTa TCT GAA GCT ATG TCA GTG-3' and its reverse complement (bases in lower case represent silent changes). The coding region of the siRNA-resistant cDNA was confirmed by DNA sequencing. Human embryonic kidney HEK 293 and HEK-293FT cells were grown in 75 cm^2 flasks in DMEM supplemented with 10% fetal bovine serum, 4mM L-glutamine and penicillin/streptomycin at 37° C and 5 % CO2. Empty vector or expression plasmid were transfected using Lipofectamine 2000 (Invitrogen).

Immunoblotting, chemiluminescence and infrared imaging

Cell lysates were boiled with equal volume of Laemmli's 2X gel loading buffer and the hot solution was loaded onto 4–20% Tris-Glycine SDS-PAGE gels (Invitrogen) to separate the proteins, followed by transfer of the proteins on to 0.45-micron nitrocellulose membrane. Membranes were blocked with TBS or PBS (pH 7.4) containing 0.1% Tween 20 and 5% nonfat dry milk (blocking buffer) and incubated overnight with primary antibodies in the same buffer. The membranes were then washed seven times for 5 minutes each with the above buffer without milk, followed by a 2-hour incubation in blocking buffer including appropriate horseradish peroxidase-conjugated secondary antibodies. Membranes were then washed as above, and the proteins detected by chemiluminescence on X-ray film using Super Signal West Dura Extended Duration Substrate (Pierce). For infrared (IR) imaging, IR-labeled secondary antibodies (dilution 1: 20,000) were used for detecting the protein signals in conjunction with the Odyssey infrared imaging system (*LI-COR, Bioscience).* Blocking and washing buffers used were same as described above, however the incubation time with the secondary antibody was half hour- one hour protected from light. For the quantification of the intensity of the protein bands membranes were dually probed, with the β-actin used as a loading control.

Lifespan and stress resistance

The lifespan and stress resistance of heterozygous *hyx/HRPT2* flies obtained by crossing *hyx/Tm3* with w^{1118} flies were examined as compared to wild type (w^{1118}) flies. Newly eclosed flies within a period of 24 hrs were collected and aged for 5 days on standard corn meal agar fly medium. Male and female flies were then separated for testing. For lifespan test, 20 flies were transferred to a vial containing 10 ml of culture medium maintained at 25 °C. Flies were transferred to fresh medium every 3 days and the number of dead flies were recorded. The survival rate per vial at each recording time was calculated by the formula: (1-[dead flies/total flies]) x 100%. Ten or more vials were used for each experiment and 3 or more independent experiments were conducted for each fly line. For data analysis, each vial was treated as a data point and analyzed by Prism software version 5.0b (GraphPad Software, Inc.). For oxidative and starvation stress tests, flies with desired genotypes eclosed within 24 hrs were collected. After ageing for 5 days flies were separated by gender and placed into vials containing Whatman paper discs (d=2.3 cm) soaked either in 350 μl of 5% sucrose solutions with or without paraquat for paraquat treatments or in H_2O for starvation tests. Five to ten vials (10 flies per vial) were used for each test and at least 3 independent experiments were performed. Dead flies were recorded daily and statistical analysis was performed using the Prism software as described above.

Chromatin immunoprecipitation assay

ChIP assay kit from Upstate (Cat. No. 17–295) was used in the analysis of HEK293 cells following the manufacturer's instructions except that the QIAquick PCR purification kit (Qiagen, Cat. No. 28104) was used for DNA purification. Purified DNA was used to amplify *CPEB1* and its flanking sequences using the following primer pairs: U1 (upstream 753 bp, ATCAAGCAAAGGCAGAGAGGGA, AAACAGACCCGACAACTGCCAA); U2

(upstream 1430 bp AGCTTCTTTGGGTTGCTGAGGT, TCCTGGAGAAAGCATGGCTCAA); U3 (upstream 2677 bp, AAACAGCCTTTGAGCCCAGCTA, TCCTGCAGAAGCACTGAACACT); S (early coding 19210 bp, TTTCACATTGAGCAGGCCGAG, ACTGTGCCTGCTTCTCCTTACA); M (middle coding 19808 bp, GGATTTCTCCAAGGTCCATGTC, TCCATGAAAGCCATCATGCCCA); D1(downstream 1105 bp, ATGTTGCTCAGGCTGGTCTCAA, TGGCTCACGCTTACAATCAGCA). The primer set, GCGCTCGTTTTGTGCAGCTTC and GTGCCCTGGCACTCATCACAC, was used to amplify the *CPEB3* gene.

Bioinformatic analysis

CPEB binds specifically to a cytoplasmic polyadenylation element (CPE) located upstream, mostly within 100 bases, of the hexanucleotide poly(A) signal (AAUAAA) sequence at the 3' UTR of mRNA to control polyadenylation of mRNAs (30). The consensus CPE has the general form: $U_{4–5}A_{1–2}U$. A PERL script was developed to identify every gene in the human RNA database that contains the conserved pattern: $U_{4–5}A_{1–2}U\ N_{1–100}$ AAUAAA where N can be any nucleotide. For quality control of the PERL script-identified genes, we randomly checked about 10% of the genes selected by the program. 100% of the individually examined genes contained the desired consensus sequence pattern. The bioinformatically-selected putative CPEB target genes were compared with potential parafibromin target genes selected by whole genome oligo microarray analysis to identify the common targets of both proteins. To evaluate the specificity of the shared targets identified by this method, each set of the targets was compared independently with a set of 3200 genes randomly selected from the NCBI Reference Sequence (RefSeq) database using Insightful-Miner (TIBCO Software, Inc.).

Supplementary Material

Refer to Web version on PubMed Central for supplementary material.

Abbreviations

CPEB	cytoplasmic polyadenylation element binding protein
HPT-JT	hyperparathyroidism-jaw tumor syndrome
ChIP	Chromatin immunoprecipitation

Acknowledgments

We are grateful to Sunita Agarwal and Stephen Marx for encouragement and helpful discussions. This research was supported by the Intramural Research Program of the National Institute of Diabetes and Digestive and Kidney Diseases.

REFERENCES

1. Jackson CE, Norum RA, Boyd SB, Talpos GB, Wilson SD, Taggart RT, et al. Hereditary hyperparathyroidism and multiple ossifying jaw fibromas: a clinically and genetically distinct syndrome. Surgery. 1990; 108:1006–1012. [PubMed: 2123361]
2. Mallette LE, Malini S, Rappaport MP, Kirkland JL. Familial cystic parathyroid adenomatosis. Ann Intern Med. 1987; 107:54–60. [PubMed: 3592449]
3. Teh BT, Farnebo F, Kristoffersson U, Sundelin B, Cardinal J, Axelson R, et al. Autosomal dominant primary hyperparathyroidism and jaw tumor syndrome associated with renal hamartomas and cystic

kidney disease: linkage to 1q21-q32 and loss of the wild type allele in renal hamartomas. J Clin Endocrinol Metab. 1996; 81:4204–4211. [PubMed: 8954016]

4. Teh BT, Farnebo F, Twigg S, Höög A, Kytölä S, Korpi-Hyövälti E, et al. Familial isolated hyperparathyroidism maps to the hyperparathyroidism-jaw tumor locus in 1q21-q32 in a subset of families. J Clin Endocrinol Metab. 1998; 83:2114–2120. [PubMed: 9626148]
5. Simonds WF, James-Newton LA, Agarwal SK, Yang B, Skarulis MC, Hendy GN, et al. Familial isolated hyperparathyroidism: Clinical and genetic characteristics of thirty-six kindreds. Medicine (Baltimore). 2002; 81:1–26. [PubMed: 11807402]
6. Simonds WF, Robbins CM, Agarwal SK, Hendy GN, Carpten JD, Marx SJ. Familial isolated hyperparathyroidism is rarely caused by germline mutation in HRPT2, the gene for the hyperparathyroidism-jaw tumor syndrome. J Clin Endocrinol Metab. 2004 Jan; 89(1):96–102. [PubMed: 14715834]
7. Carpten JD, Robbins CM, Villablanca A, Forsberg L, Presciuttini S, Bailey-Wilson J, et al. HRPT2, encoding parafibromin, is mutated in hyperparathyroidism-jaw tumor syndrome. Nat Genet. 2002 Dec; 32(4):676–680. [PubMed: 12434154]
8. Shattuck TM, Valimaki S, Obara T, Gaz RD, Clark OH, Shoback D, et al. Somatic and germ-line mutations of the HRPT2 gene in sporadic parathyroid carcinoma. N Engl J Med. 2003 Oct 30; 349(18):1722–1729. [PubMed: 14585940]
9. Cetani F, Pardi E, Borsari S, Viacava P, Dipollina G, Cianferotti L, et al. Genetic analyses of the HRPT2 gene in primary hyperparathyroidism: germline and somatic mutations in familial and sporadic parathyroid tumors. J Clin Endocrinol Metab. 2004 Nov; 89(11):5583–5591. [PubMed: 15531515]
10. Rozenblatt-Rosen O, Hughes CM, Nannepaga SJ, Shanmugam KS, Copeland TD, Guszczynski T, et al. The parafibromin tumor suppressor protein is part of a human Paf1 complex. Mol Cell Biol. 2005 Jan; 25(2):612–620. [PubMed: 15632063]
11. Yart A, Gstaiger M, Wirbelauer C, Pecnik M, Anastasiou D, Hess D, et al. The HRPT2 tumor suppressor gene product parafibromin associates with human PAF1 and RNA polymerase II. Mol Cell Biol. 2005 Jun; 25(12):5052–5060. [PubMed: 15923622]
12. Zhu B, Mandal SS, Pham AD, Zheng Y, Erdjument-Bromage H, Batra SK, et al. The human PAF complex coordinates transcription with events downstream of RNA synthesis. Genes Dev. 2005 Jul 15; 19(14):1668–1673. [PubMed: 16024656]
13. Mosimann C, Hausmann G, Basler K. Parafibromin/Hyrax activates Wnt/Wg target gene transcription by direct association with beta-catenin/Armadillo. Cell. 2006 Apr 21; 125(2):327–341. [PubMed: 16630820]
14. Lin L, Czapiga M, Nini L, Zhang JH, Simonds WF. Nuclear localization of the parafibromin tumor suppressor protein implicated in the hyperparathyroidism-jaw tumor syndrome enhances its proapoptotic function. Mol Cancer Res. 2007 Feb; 5(2):183–193. [PubMed: 17314275]
15. Woodard GE, Lin L, Zhang JH, Agarwal SK, Marx SJ, Simonds WF. Parafibromin, product of the hyperparathyroidism-jaw tumor syndrome gene HRPT2, regulates cyclin D1/PRAD1 expression. Oncogene. 2005 Feb 10; 24(7):1272–1276. [PubMed: 15580289]
16. Zhang C, Kong D, Tan MH, Pappas DL Jr, Wang PF, Chen J, et al. Parafibromin inhibits cancer cell growth and causes G1 phase arrest. Biochem Biophys Res Commun. 2006 Nov 10; 350(1):17–24. [PubMed: 16989776]
17. Lin L, Zhang JH, Panicker LM, Simonds WF. The parafibromin tumor suppressor protein inhibits cell proliferation by repression of the c-myc proto-oncogene. Proc Natl Acad Sci U S A. 2008 Nov 11; 105(45):17420–17425. [PubMed: 18987311]
18. Rozenblatt-Rosen O, Nagaike T, Francis JM, Kaneko S, Glatt KA, Hughes CM, et al. The tumor suppressor Cdc73 functionally associates with CPSF and CstF 3' mRNA processing factors. Proc Natl Acad Sci U S A. 2009 Jan 20; 106(3):755–760. [PubMed: 19136632]
19. Greenspan, RJ. Fly Pushing: The Theory and Practice of Drosophila Genetics. Cold Spring Harbor, NY: Cold Spring Harbor Laboratory Press; 1997. Chapter 4. Synthesizing specific genotypes; p. 63-86.
20. Singh A, Shi X, Choi KW. Lobe and Serrate are required for cell survival during early eye development in Drosophila. Development (Cambridge, England). 2006 Dec; 133(23):4771–4781.

21. Chern JJ, Choi KW. Lobe mediates Notch signaling to control domain-specific growth in the Drosophila eye disc. Development (Cambridge, England). 2002 Sep; 129(17):4005–4013.
22. Groisman I, Ivshina M, Marin V, Kennedy NJ, Davis RJ, Richter JD. Control of cellular senescence by CPEB. Genes Dev. 2006 Oct 1; 20(19):2701–2712. [PubMed: 17015432]
23. Lasko P. Gene regulation at the RNA layer: RNA binding proteins in intercellular signaling networks. Sci STKE. 2003 Apr 22.2003(179):RE6. [PubMed: 12709531]
24. Richter JD. CPEB: a life in translation. Trends Biochem Sci. 2007 June; 32(6):279–285. [PubMed: 17481902]
25. Reifegerste R, Moses K. Genetics of epithelial polarity and pattern in the Drosophila retina. BioEssays. 1999 Apr; 21(4):275–285. [PubMed: 10377890]
26. Campisi J, d'Adda di Fagagna F. Cellular senescence: when bad things happen to good cells. Nat Rev Mol Cell Biol. 2007 Sep; 8(9):729–740. [PubMed: 17667954]
27. Mueller CL, Jaehning JA. Ctr9, Rtf1, and Leo1 are components of the Paf1/RNA polymerase II complex. MolCellBiol. 2002; 22:1971–1980.
28. Campisi J. Senescent cells, tumor suppression, and organismal aging: good citizens, bad neighbors. Cell. 2005 Feb 25; 120(4):513–522. [PubMed: 15734683]
29. Campisi J. Aging, tumor suppression and cancer: high wire-act! Mech Ageing Dev. 2005 Jan; 126(1):51–58. [PubMed: 15610762]
30. Mendez R, Richter JD. Translational control by CPEB: a means to the end. Nat Rev Mol Cell Biol. 2001 Jul; 2(7):521–529. [PubMed: 11433366]
31. Burns DM, Richter JD. CPEB regulation of human cellular senescence, energy metabolism, and p53 mRNA translation. Genes Dev. 2008 Dec 15; 22(24):3449–3460. [PubMed: 19141477]
32. Nordick K, Hoffman MG, Betz JL, Jaehning JA. Direct interactions between the Paf1 complex and a cleavage and polyadenylation factor are revealed by dissociation of Paf1 from RNA polymerase II. Eukaryot Cell. 2008 Jul; 7(7):1158–1167. [PubMed: 18469135]
33. Barnard DC, Ryan K, Manley JL, Richter JD. Symplekin and xGLD-2 are required for CPEB-mediated cytoplasmic polyadenylation. Cell. 2004 Nov 24; 119(5):641–651. [PubMed: 15550246]
34. Dunlop EA, Tee AR. Mammalian target of rapamycin complex 1: signalling inputs, substrates and feedback mechanisms. Cell Signal. 2009 Jun; 21(6):827–835. [PubMed: 19166929]

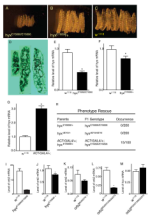

Fig 1. *Hyrax/HRPT2* is essential for normal larval development in *Drosophila* and is upstream of the cytoplasmic polyadenylation element-binding protein (CPEB) homolog *Orb2*

The morphology of second instar larvae were compared between hyx^{EY6898} homozygous and heterozygous mutants and wild type flies by stereomicroscopy (A–C) and hematoxylin and eosin histological staining (D). Shown in D., left to right, are longitudinal sections of hyx^{EY6898} homozygous and heterozygous mutants and w^{1118} larvae. The transcript levels of *hyx/HRPT2* were measured by qRT-PCR in both hyx^{EY6898} homozygous second instar larvae (E) and heterozygous adult (F) flies. Rescue of the hyx^{EY6898} homozygous lethal phenotype was performed with an actin promoter-controlled GAL4 driven overexpression of the *hyx/HRPT2* gene from the hyx^{EY6898} allele (G–H). For comparison, results with the hyx^{dEY2} excision mutant are also shown (H). Expression of the *orb2* gene in hyx^{EY6898} homozygous larvae and heterozygous adult flies (I–J) and adult $orb2^{BG02373}$ heterozygous and homozygous flies (K–L), and *hyx/HRPT2* gene expression in $orb2^{BG02373}$ homozygous mutant flies (M) was quantified by qRT-PCR. For morphology experiments, at least 50 second instar larvae were examined for each genotype. All qRT-PCR data were from at least 9 data points comprising at least three independent biological repeats.

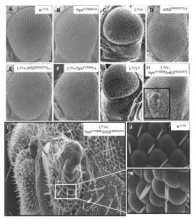

Figure 2. Genetic interaction among *lobe/Akt1s1, hyx/HRPT2* and *orb2/CPEB* evident from *Drosophila* eye phenotypes

Genetic interactions of flies were recognized by formation of novel notch and overgrowth (NOG) structures at the ventral part of eye after crosses between flies with different genotypic backgrounds. Shown are representative eye phenotypes captured by scanning electron microscopy for wild type (A), heterozygous hyx^{EY6898} mutant of *hyx/HRPT2* (B), heterozygous L^{si} mutant of *lobe/AKT1S1* (C), heterozygous $orb2^{BG02373}$ mutant of *orb2/CPEB* (D); double heterozygous mutants of *lobe* and *orb2* (E), *lobe* and *hyx/HRPT2* (F); homozygous *lobe* L^{si} mutant (G) and triple heterozygous hybrid mutants of *lobe*, *hyx/HRPT2* and *orb2* genes (H). Higher magnification image of boxed region of H is shown in I. The ommatidia and sensory bristle phenotype of the triple heterozygous *lobe*, *hyx/HRPT2* and *orb2* mutant are shown (I, K). Higher magnification image of boxed region of I is shown in K, with wild type shown for comparison (J).

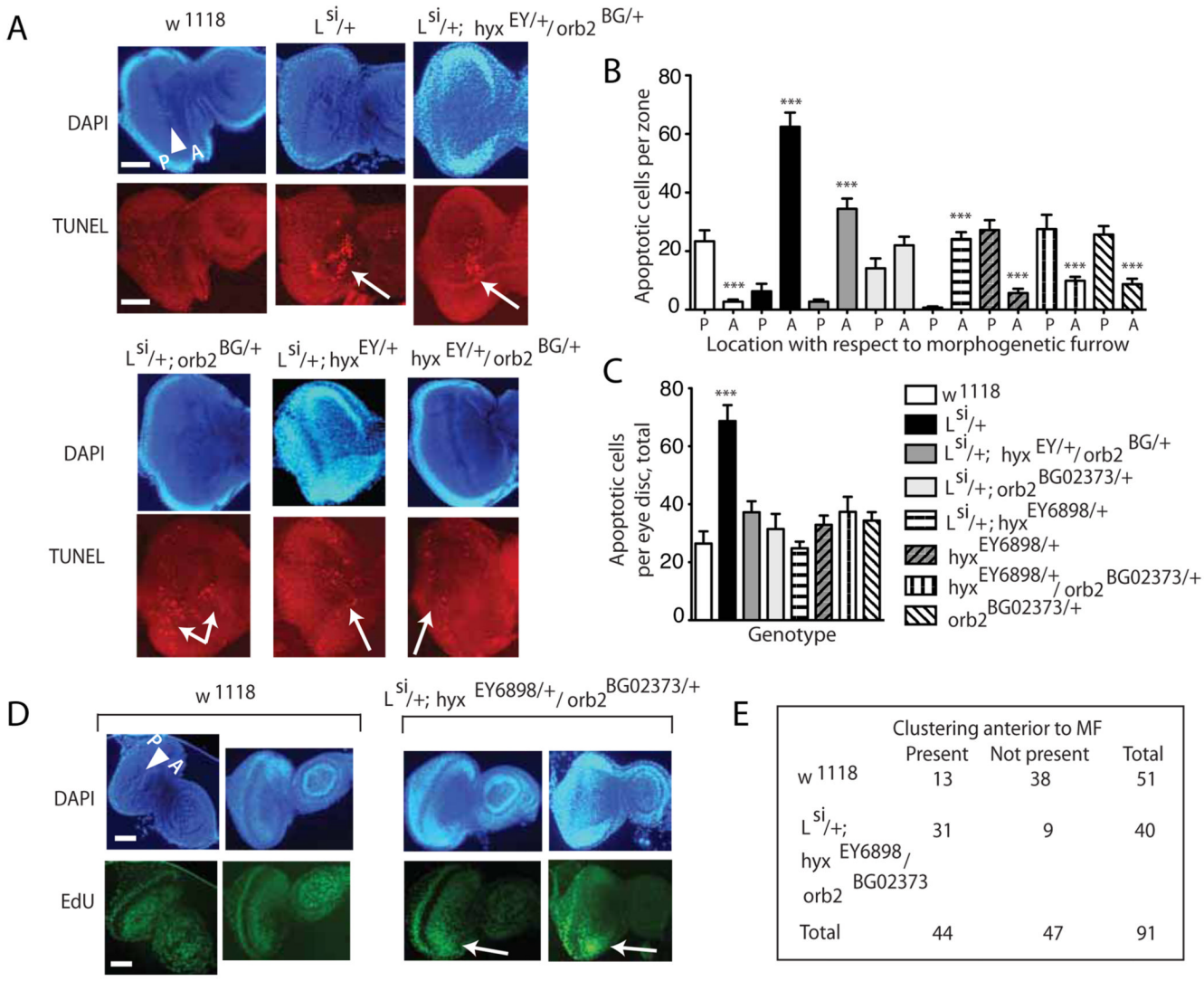

	Clustering anterior to MF		
	Present	Not present	Total
w 1118	13	38	51
L si/+; hyx EY6898/ orb2 BG02373	31	9	40
Total	44	47	91

Figure 3. The imaginal eye disc of triply heterozygous mutant L^{si}/+; hyx^{EY6898}/$orb2^{BG02373}$ larvae is characterized by an abnormal pattern of apoptosis and increased ectopic cellular proliferation

A. DAPI nuclear staining (upper) and TUNEL analysis (lower) of the eye imaginal discs of wild-type, L^{si}/+, L^{si}/+; $hyx^{EY6898/+}$/$orb2^{BG02373/+}$ triple heterozygote, and L^{si}/+; $hyx^{EY6898/+}L^{si}$/+; $orb2^{BG02373/+}$, and $hyx^{EY6898/+}$;$orb2^{BG02373/+}$ double heterozygote third instar larvae. White triangle indicates the morphogenetic furrow (MF), with anterior (A) and posterior (P) directionality indicated. Scale bar = 1 mm. Please note that in the legend to A. (and in the legend in C. for the triple heterozygote) the genotype for $hyx^{EY6898/+}$ is abbreviated $hyx^{EY/+}$ and the genotype for $orb2^{BG02373/+}$ is abbreviated to $orb2^{BG/+}$**B**. The majority of apoptotic cell nuclei in the wild-type, $hyx^{EY6898/+}orb2^{BG02373/+}$, and $hyx^{EY6898/+}$/$orb2^{BG02373/+}$ eye discs were located posterior (P) to the MF and uniformly distributed whereas the majority of apoptotic nuclei in the L^{si}/+ heterozygotes and L^{si}/+; $hyx^{EY6898/+}$/$orb2^{BG02373/+}$ triple heterozygotes are found anterior (A) to the MF and grouped in large clusters (white arrows in figure part A.). The majority of apoptotic nuclei in the L^{si}/+; $hyx^{EY6898/+}$ double heterozygotes are also localized anterior to the MF, but are dispersed rather than grouped (***, p <0.0001, anterior vs. posterior, 2-tailed t test). There

was no significant difference in the anterior and posterior distribution of apoptotic nuclei in $L^{si}/+$; $orb2^{BG02373/+}$ double heterozygotes (p=0.08, anterior vs. posterior, 2-tailed t test). Legend as in C. **C**. The total number of TUNEL-positive apoptotic nuclei per eye disc in $L^{si}/+$ heterozygotes is significantly increased compared to wild-type, triple, double and other single heterozygotes (***, p <0.0001, $L^{si}/+$ vs. wt or double, triple or other single heterozygotes, 2-tailed t test). For B. and C. the number of distinct eye imaginal discs counted: wt, n= 20; $L^{si}/+$, n= 22; $L^{si}/+$; $hyx^{EY6898/+}/orb2^{BG02373/+}$ triple heterozygotes, n= 42; $L^{si}/+$; $orb2^{BG02373/+}$, n=19; $L^{si}/+$; $hyx^{EY6898/+}$, n=20; $hyx^{EY6898/+}$, n=16; $orb2^{BG02373/+}$, n=16; $hyx^{EY6898/+}$; $orb2^{BG02373/+}$, n=16. **D**. Third instar larvae eye discs of wild-type and $L^{si}/+$; $hyx^{EY6898}/orb2^{BG02373}$ triple heterozygotes with nuclei stained with DAPI (upper) and proliferating cells stained for the incorporation of the nucleoside 5-ethynyl-2´-deoxyuridine (EdU) (lower) as described in Materials and Methods. Labels in DAPI images as in A. White arrows indicate bright clusters of proliferating cells anterior to MF. **E**. 2 × 2 contingency table showing the number of wild-type and triple heterozygote eye discs in which bright clusters of proliferating cells anterior to the MF were observed, scored as described in Materials and Methods (n = 51 for wild-type, n = 40 for triple heterozygotes; Fisher's exact test, 2-tailed p value <0.0001).

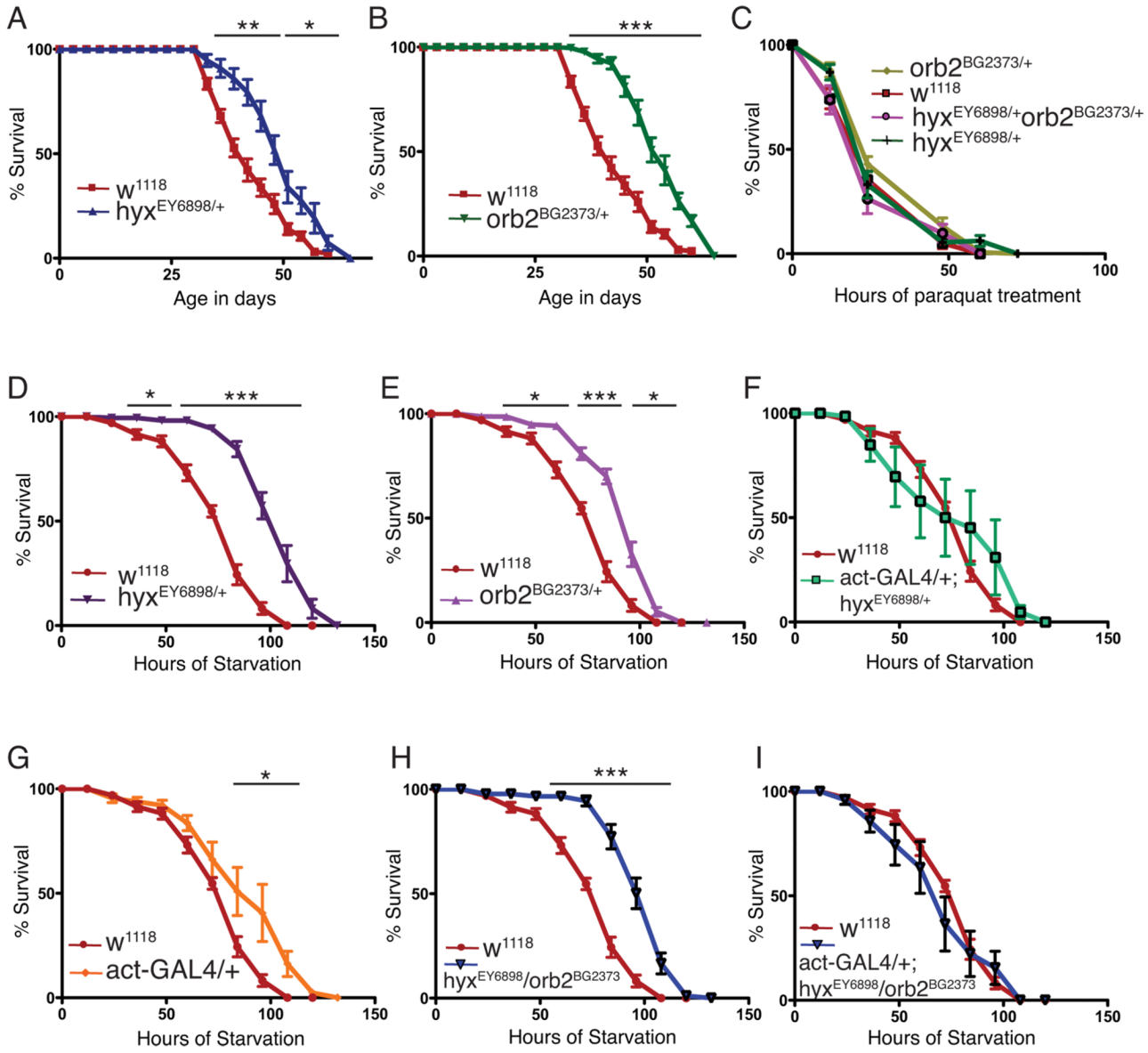

Figure 4. Enhanced longevity and starvation resistance in *hyx/HRPT2* and *Orb2/CPEB* mutant flies

The longevity of the indicated heterozygous *hyx /HRPT2* and *orb2* mutant flies were examined under standard culture conditions as compared to wild type flies (A and B). Survival upon exposure to the herbicide and oxygen free radical–generator paraquat of wild-type and the indicated mutant flies is shown (C). Flies in C were fed with a paraquat-sucrose solution. Survival upon starvation (D–I) of the indicated single or double *hyx/HRPT2* and *orb2* heterozygous mutants is shown. Flies in D-I were supplied only with water to test starvation resistance. Experiments aimed at the rescue of the hyx^{EY6898} enhancer trap mutant by mating with a driver strain expressing *GAL4* from the *5C-actin* promoter (*act-GAL4*) are shown in F and I, with the driver-only control shown in G. The number of surviving flies was recorded every three days for lifespan tests and daily for stress tests. Ten or more vials were used for each experiment and 3 or more independent experiments were conducted for each fly line. Vials contained 20 flies each for lifespan determination and 10 flies each for

stress tests. Each data point shown represents the pooled mean survival from 10 to 12 vials of the indicated genotype, except for the w^{1118} flies used in stress testing in which each data point represents the pooling of 20 vials (*, $p < 0.05$; **, $p < 0.001$; ***, $p < 0.0001$; vs. wt for the indicated time points, 2-tailed t test).

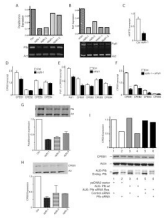

Figure 5. Knockdown of parafibromin impairs *CPEB1* expression at the transcriptional level

The expression of *HRPT2, Paf1* and *CPEB1-4* genes in human embryonic kidney cells after RNA interference employing siRNAs targeting *HRPT2* (*sipfb*) and *Paf1 (sipaf1)* as analyzed by immunoblotting using infrared imaging or quantitative RT-PCR is shown. (A) and (B): expression of parafibromin and Paf1 protein by immunoblot (lower panels) and quantification the indicated bands normalized to the actin (Act) loading control by infrared imaging (upper). (C), (D), (E) and (F): transcript levels of the *HRPT2, Paf1*, and *CPEB1-4* genes in *HRPT2*- and/or *Paf1*-siRNA treated and control siRNA-treated cells were measured by quantitative RT-PCR. (*, $p < 0.05$; **, $p < 0.005$ vs. control transcript level, 2-tailed t-test) (G) and (H): immunoblot analysis of parafibromin (Pfb) and CPEB1 protein expression in control or *HRPT2*-siRNA treated cells (insets) with lower histograms showing quantification of expression relative to actin based on infrared imaging of immunoblots. (I): expression of CPEB1 in cells transfected with the empty pcDNA3 vector only, wild-type AU5 epitope-tagged parafibromin cDNA, AU5 epitope-tagged parafibromin cDNA engineered with silent base changes to render it resistant to siPfb-1 siRNA, and either control siRNA or siPfb-1 siRNA, as indicated, was determined by immunoblot (lower panels) and quantified relative to actin, by infrared imaging of immunoblots (upper graph). Experiments shown in A, B, G and H used HEK-293FT cells, while the experiments shown in C, D, E, F, and I used HEK-293 cells. For qRT-PCR each repeat employed triplicate reactions and each data set represents an n= 9 or more. All experiments are representative of three or more independent biological repeats.

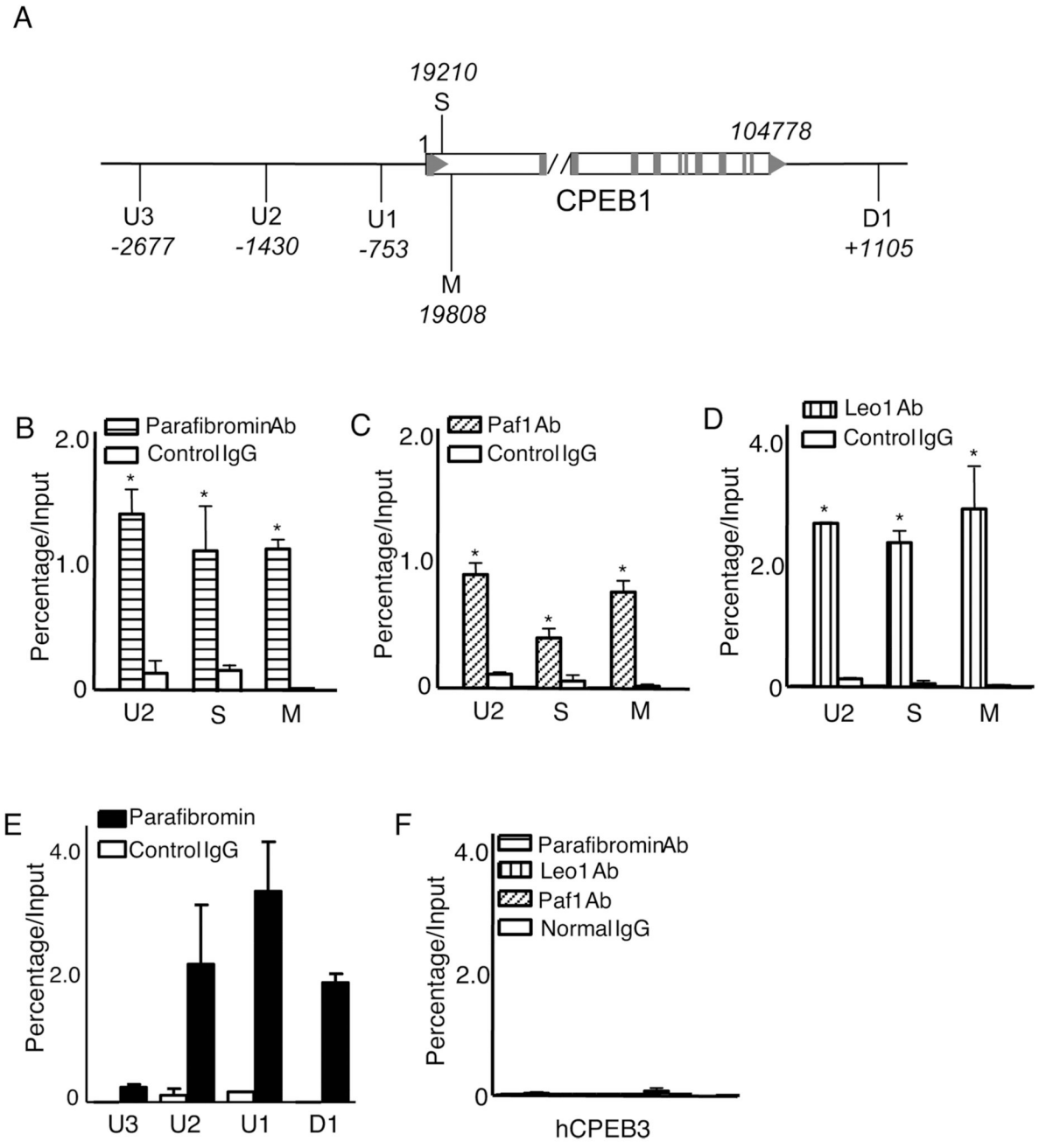

Figure 6. Chromatin immunoprecipitation demonstrates occupancy at *CPEB1* but not *CPEB3* by the PAF1 complex

The physical association of endogenous parafibromin and other components of the PAF1 complex (including the Paf1 and Leo1 proteins) with the human *CPEB1* promoter was examined by ChIP in HEK293 cells. (A) Schematic diagram showing the relative location of PCR primer sets employed in the ChIP assay along the human *CPEB1* gene and flanking regions (not to scale). The negative numbers associated with U1-U3 indicate upstream position (in bp) of the primer sets relative to transcription start site, the positive number associated with D1 indicates downstream position (in bp) of the primer set relative to the end of the final gene exon. The neutral numbers associated with the early coding sequence

(S) and middle coding sequence (M) represent the internal positions (in bp) of the primer sets 3' to the transcription start site. (B–D): ChIP analysis using primer sets targeting upstream (U2), early coding (S) and middle coding (M) sequence of *CPEB1* using either control IgG or antibodies against parafibromin (B), Paf1 (C) and Leo1 (D) proteins as shown. (E) ChIP analysis of parafibromin occupancy of regions upstream or the *CPEB1* transcription start site or downstream of the end of the gene using the indicated primer sets. (F) ChIP analysis of the parafibromin, Paf1 and Leo1 occupancy of the human *CPEB3* gene using the same ChIPed cell lysates employed in B-E. All experiments are representative of three or more independent biological repeats.

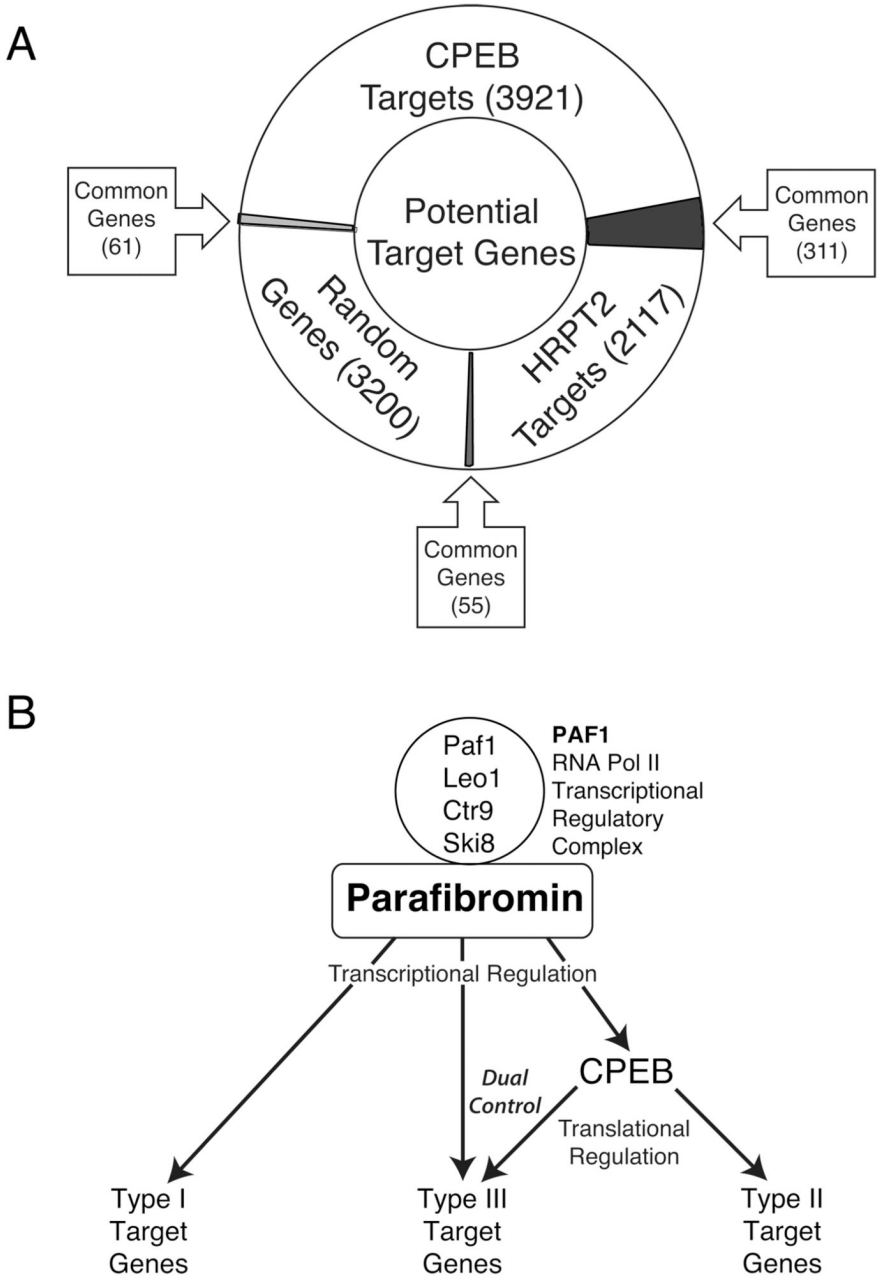

Figure 7. Bioinformatic analysis of potential *HRPT2* and *CPEB* targets suggests duel level of parafibromin gene control

(A) Diagram showing the relationship of potential gene targets of *HRPT2* and *CPEB1* genes, and a set of randomly chosen genes. Potential *HRPT2* targets (2117 genes) were identified by whole genome oligo microarray analysis comparing pools of transcript from HEK293 cells treated with either *HRPT2*-specific or scrambled control siRNA. Potential *CPEB1* targets (3921 genes) were identified from the human genomic database based on the presence of a potential CPE consensus sequence in the 3' untranslated region. To assess the specificity of the overlapping set of common *HRPT2* and *CPEB1* target genes, both pools of *HRPT2* and *CPEB1* potential target genes were also compared to a set of 3200 randomly-

selcted human genes. An arrowed square box indicates the overlap identified by each of the three pairings (Fisher's exact test, 2-tailed p value < 0.002, *HRPT2/CPEB* vs. *HRPT2*/Random; < 0.01, *CPEB/HRPT2* vs. *CPEB*/Random). (B) Model illustrating three types of potential targets of parafibromin in association with PAF1 transcriptional regulatory complex: type I, regulated only transcriptionally (e.g. genes identified by whole genome oligo microarray analysis, not including the genes overlapping with *CPEB1* targets); type II, regulated indirectly at the level of translation through *CPEB1* (e.g. genes identified by CPE consensus sequence analysis, not including the genes overlapping with *HRPT2* targets); and type III, regulated dually by transcription and indirectly by translational effects via *CPEB1* (e.g. genes common to both *HRPT2* and *CPEB1* target gene pools). This model of dual regulation does not exclude the additional possibility of CPEB regulation by parafibromin involving direct physical complex formation, since the CPEB-binding scaffolding protein symplekin has been found in anti-parafibromin immunoprecipitates (18).

Table I

Genetic Interactions of Selected Genes

Parents			F1 Genotype	% Flies with NOG[a] eye phenotype	Molecular Function
Parent 1	**Parent 2**	**No. of Crosses**			
$L^{si}/+$	W^{1118}	1	$L^{si}/+^{b}$	0	L is the fly homolog of mammalian AKT1S1
	$hyx^{EY6898}/+$	2	$L^{si}/+$; $hyx^{EY6898}/+$	0	Hyx is the fly homolog of parafibromin, a component of PAF1 complex associated with RNA polymerase II
$hyx^{EY6898}/+$	W^{1118}	3	$hyx^{EY6898}/+$	0	
$L^{si}/+;hyx^{EY6898}/+$	$orb2^{BG02373}/+$	4	$L^{si}/+;hyx^{EY6898}/orb2^{BG02373}$	23	Orb and Orb2 are homologs of human CPEB, a component of the eIF-4E translation initiation complex, regulating polyadenylation of certain mRNAs
			$L^{si}/+;orb2^{BG02373}/+$	6	
	$orb2^{Scf\text{-}R6}/+$	5	$L^{si}/+;hyx^{EY6898}/orb2^{Scf\text{-}R6}$	26	
			$L^{si}/+;orb2^{Scf\text{-}R6}/+$	4	
	$orb2^{Scf\text{-}R11}/+$	6	$L^{si}/+;hyx^{EY6898}/orb2^{Scf\text{-}R11}$	12	
			$L^{si}/+;orb2^{Scf\text{-}R11}/+$	0	
	$orb^{dec}/+$	7	$L^{si}/+;hyx^{EY6898}/orb^{dec}$	2	
			$L^{si}/+;orb^{dec}/+$	0	
	$orb^{EY08547}/+$	8	$L^{si}/+;hyx^{EY6898}/orb^{EY08547}$	0	
			$L^{si}/+;orb^{EY08547}/+$	0	
	$orb^{Exel6274}/+$	9	$L^{si}/+;hyx^{EY6898}/orb^{Exel6274}$	21	
			$L^{si}/+;orb^{Exel6274}/+$	0	
	$orb^{Exel6280}/+$	10	$L^{si}/+;hyx^{EY6898}/orb^{Exel6280}$	6	
			$L^{si}/+;orb^{Exel6280}/+$	0	
	$atu^{s1938}/+$	11	$L^{si}/+;hyx^{EY6898}/atu^{s1938}$	33	Atu, Atms, and dCtr9 are the fly homologs of Leo1, Paf1 and Ctr9 respectively, components of the PAF1 complex
			$L^{si}/+;atu^{s1938}/+$	0	
	$atms^{NP5451}/+$	12	$L^{si}/+;hyx^{EY6898}/atms^{NP5451}$	23	
			$L^{si}/+;atms^{NP5451}/+$	0	
	$atms^{rk509}/+$	13	$L^{si}/+;hyx^{EY6898}/atms^{rk509}$	46	

Parents			F1 Genotype	% Flies with NOG[a] eye phenotype	Molecular Function
Parent 1	Parent 2	No. of Crosses			
			$L^{si}/+;atms^{rk509}/+$	19	
	$dctr9^{NP5197}/+$	14	$L^{si}/+;hyx^{EY6898}/dctr9^{NP5197}$	25	
			$L^{si}/+;dctr9^{NP5197}/+$	0	
	ArmG0192	20	$Arm^{G0192}/+;L^{si}/+;hyx^{EY6898}/+$	12	Arm (Armadillo) is WNT signaling pathway component
			$Arm^{G0192}/+;L^{si}/+;+/+$	0	
	$4EBP^{k10101}$	21	$L^{si}/4EBP^{k10101};hyx^{EY6898}/+$	0	Components of Foxo signaling pathway
			$L^{si}/4EBP^{k10101};+/+$	0	
	$4EBP^{06270}$	22	$L^{si}/4EBP^{06270};hyx^{EY6898}/+$	0	
			$L^{si}/4EBP^{06270};+/+$	0	
	$4EBP^{k13506}$	23	$L^{si}/4EBP^{k13506};hyx^{EY6898}/+$	0	
			$L^{si}/4EBP^{k13506};+/+$	0	
	$4EBP^{EY00763}$	24	$L^{si}/4EBP^{EY00763};hyx^{EY6898}/+$	0	
			$L^{si}/4EBP^{EY00763};+/+$	0	
	$Foxo^{ED5634}$	25	$L^{si}/+;hyx^{EY6898}/Foxo^{ED5634}$	0	
			$L^{si}/+;Foxo^{ED5634}/+$	0	
	$Foxo^{DG02610}$	26	$L^{si}/+;hyx^{EY6898}/Foxo^{DG02610}$	0	
			$L^{si}/+;Foxo^{DG02610}/+$	0	
	$Foxo^{EY16506}$	27	$L^{si}/+;hyx^{EY6898}/Foxo^{EY16506}$	0	
			$L^{si}/+;Foxo^{EY16506}/+$	0	
	$Foxo^{BG01018}$	28	$L^{si}/+;hyx^{EY6898}/Foxo^{BG01018}$	0	
			$L^{si}/+;Foxo^{BG01018}/+$	0	
	$Foxo^{EY11248}$	29	$L^{si}/+;hyx^{EY6898}/Foxo^{EY11248}$	0	
			$L^{si}/+;Foxo^{EY11248}/+$	0	
	$Foxo^{ED5644}$	30	$L^{si}/+;hyx^{EY6898}/Foxo^{ED5644}$	0	
			$L^{si}/+;Foxo^{ED5644}/+$	0	

[a] NOG: Notch and Overgrowth, with notches and variably sized dysplastic cornlike overgrowths in the ventral eye fields

[b] Typical $L^{si/+}$ phenotype is absence of ventral eye fields